

# Chapter 2

## Structural Characterization of Inorganic Biomaterials

Irene M. Mavridis

### Contents

2.1	Introduction .....	20
2.2	Diffraction and Scattering Methods .....	21
2.2.1	Single-Crystal X-Ray Diffraction .....	21
2.2.2	Powder X-Ray Diffraction .....	22
2.2.3	Small-Angle Scattering .....	24
2.2.4	Grazing Incidence X-Ray Diffraction .....	25
2.2.5	Fiber Diffraction .....	26
2.2.6	Electron Diffraction .....	28
2.3	Microscopy .....	30
2.3.1	Transmission Electron Microscopy .....	30
2.3.2	Scanning Electron Microscopy .....	31
2.3.3	Confocal Scanning Laser Microscopy .....	31
2.3.4	Atomic Force Microscopy .....	32
2.4	Spectroscopy .....	32
2.4.1	Infrared Spectroscopy (IR) .....	32
2.4.2	Raman Spectroscopy .....	33
2.4.3	Nuclear Magnetic Resonance Spectroscopy .....	33
2.5	Thermal Analysis .....	34
2.6	Concluding Remarks .....	35
	References .....	37

**Abstract** Composite materials with unique architectures are ubiquitous in nature, e.g., marine shells, sponge spicules, bones, and dentine. These structured organic–inorganic systems are generated through self-assembly of organic matter (usually proteins or lipids) into scaffolds, onto which the inorganic component is deposited in organized hierarchical structures of sizes spanning several orders of magnitude. The development of bio-inspired materials is possible through the

---

I.M. Mavridis (✉)  
National Center for Scientific Research Demokritos, Aghia Paraskevi, P. O. Box 60228,  
Athens, Greece  
e-mail: [mavridi@chem.demokritos.gr](mailto:mavridi@chem.demokritos.gr)

design of synthetic bottom-up self-assembly methods. Knowledge of the structure is required in order to assess the efficiency of their design and evaluate their properties. This chapter reviews the main methods used for structure determination of natural and synthetic inorganic biomaterials, namely, X-ray diffraction and scattering and electron diffraction and microscopy (TEM, SEM), as well as the AFM and CSLM microscopy methods. Moreover, spectroscopic (IR, NMR, and Raman) and thermal methods are presented. Examples of biomimetic synthetic materials are used to show the contribution of single or multiple techniques in the elucidation of their structure.

## 2.1 Introduction

Molecular recognition and self-assembly are well-known chemical and biological processes leading to selectivity, binding, and special functions, e.g., transport of molecules. Molecular recognition involves geometrical and energetic complementarities between molecular species. The geometric complementarity in chemistry has been recognized early by Fischer (1894) as the “lock and key” principle, but it was only in the late 1970s that the concept gained momentum in connection with supramolecular chemistry (Lehn 1995). It is recognized that high specificity of a molecular system A towards another B in the presence of other related species is achieved by complementarity in shape and size between A and B and multiple intermolecular nonbonding interactions, such as H-bonds and dipole–dipole, resulting in large contact areas and large difference in the binding free energy between A and B (Lehn 1995). Self-assembly by molecular recognition leads to unique architectures in nature that most of the time serve the purpose of specific physical and chemical functions. These structures are organic–inorganic composite materials generated through the self-assembly of organic matter (usually proteins or lipids, 1–100 nm) acting as frameworks that through molecular recognition generate orientation and deposition of the inorganic component in an organized manner. The overall structure is hierarchical with size scales ranging from the nano (nm) to the macro (cm) scale. Some examples relevant to this chapter are (a) sponge spicules comprising a proteinaceous axial filament and amorphous hydrated silica deposited concentrically around it; (b) marine shells, such as nacre of abalone, composed of films (<10 nm) of silk-like proteins,  $\beta$ -chitin, and inorganic aragonite ( $\text{CaCO}_3$ ) platelets (<500 nm); (c) bone, a very diverse and complex tissue, which can be described in simplified terms as comprising an organic component, mainly of type 1 collagen, and a mineralized inorganic component of carbonated apatite platelets; and (d) dentin, the bone-like matrix between the exterior enamel and the pulp of the tooth, composed also of inorganic and organic materials (mainly hydroxyapatite and collagen) structured in closely packed “dentinal tubules.”

By mimicking nature’s way, it is possible to design and synthesize hierarchically structured materials for various uses, especially for biomedical purposes, as, for example, the much-needed bone tissue regeneration. Detailed structural

determination is required in order to monitor how close any synthetic biomaterial resembles its prototype. Moreover, it permits to assess the design of their synthesis, usually by synthetic bottom-up self-assembly methods, to get insight in the mechanism of formation and evaluate their properties, so that the biomimetic approach converges to the natural one in a self-consistent way. The modern methods available for analysis of the structure are very powerful, which has contributed greatly to the advancement of material science and the development of biomimetic materials.

## 2.2 Diffraction and Scattering Methods

### 2.2.1 Single-Crystal X-Ray Diffraction

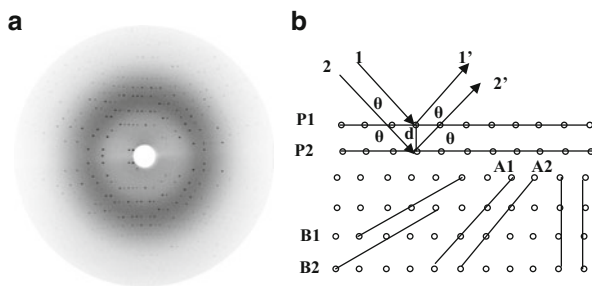
The scattering of X-rays by single crystals (continuous and infinite 3-dimensional lattice) generates diffraction, which has been used to determine the structure of matter, since the beginning of the twentieth century. The method, known as X-ray crystallography, provides the detailed atomic positions of any examined substance in its crystal lattice (Blow 2002). However, in order to obtain this detailed information, single crystals are required. The inorganic biomaterials, as composite materials of more than one species and/or phases, cannot form single crystals, although parts of them can be polycrystalline and some parts frequently exhibit order of some degree. The presentation of the single crystal diffraction that follows will help the discussion of the diffraction methods used for inorganic biomaterials, which is that of polycrystalline or low-order materials. Figure 2.1 shows a diffraction image by a single crystal, each single spot corresponding to a unique diffraction direction  $hkl$  in space. Bragg gave a simplified picture of diffraction describing it as reflection of X-rays by infinite sets of equivalent planes P, A, B, etc. (infinite number in every set) of the crystal lattice. Each set of planes is characterized by a unique direction and interplanar spacing  $d_{hkl}$ . If a parallel X-ray beam (1, 2 in Fig. 2.1) falls on any set of planes P, diffraction occurs (1', 2' in Fig. 2.1) only if the planes P form the same angle  $\theta_{hkl}$  with the incident beam and the diffracted beam (reflection condition). Thus, each diffraction direction  $hkl$  (called “reflection”) corresponding to the unique crystal spacing  $d_{hkl}$  is related to the diffraction angle  $\theta_{hkl}$  according to the well-known Bragg’s law:

$$2d_{hkl} \sin \theta_{hkl} = n_{hkl} \lambda \quad (2.1)$$

where  $\lambda$  is the wavelength of the radiation and  $n$  is an integer corresponding the order of the “reflection.”

X-ray diffraction, the most commonly used method to examine the molecular structure, depends on the scattering of X-rays by the electron density of atoms and molecules. Neutron radiation can also be used to determine the molecular structure by the same techniques. The neutron beam, depending on scattering by the nuclei,

**Fig. 2.1** Single-crystal X-ray diffraction image (a); schematic diagram of Bragg's law (b)



has scattering cross section approximately equal for most atoms, in contrast to this of X-rays that increases with atomic number. Therefore, neutron diffraction techniques are more sensitive to lighter atoms, e.g., it is ideal to detect hydrogen bonding in biological systems. However, neutron diffraction generally requires large crystals, which are not readily available.

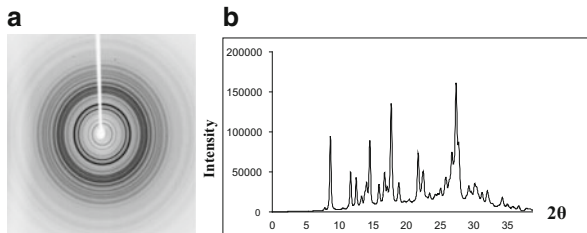
For substances for which it is difficult to obtain single crystals, notably proteins and other biological systems, disordered or low-order materials, ceramics, or macromolecules, other methods are used, such as small-angle X-ray scattering, fiber diffraction, and powder X-ray diffraction (XRD).

### 2.2.2 Powder X-Ray Diffraction

A polycrystalline powder comprises grains of single crystals in all orientations; thus, the diffraction reduces to concentric circles, each characterized by a specific  $\theta$  angle (Fig. 2.2) and a unique set of spacing according to Bragg's law (Klug and Alexander 1974). The pattern provides the fingerprint of polycrystalline inorganic materials, due to the fact that each mineral has a unique lattice and set of  $d$ -spacings. Determination of all  $d$ -spacings from the powder XRD data (all peaks in the diagram of Fig. 2.2) by Bragg's law provides identification of the inorganic materials by comparison with known standards or with the help of databases, as the International Centre for Diffraction Data, which stores a huge amount of XRD patterns. The use of the latter is facilitated by automated search/match routines.

Powder XRD is used (a) to determine the lattice parameters (unit cell of crystal) and the symmetry of the lattice, thus to determine the phase of the material; (b) to detect if a sample is a mixture of more than one crystalline compound; (c) to detect and monitor phase transitions, as these are characterized by change of the lattice, therefore change of the diffraction pattern; (d) to calculate thermodynamic parameters as thermal expansion, which can be observed from change of the  $2\theta$  angle of diffraction peaks with the change of temperature, resulting from expansion or contraction of lattice parameters; (e) to give information on the degree of crystallinity or the crystallite size for fine-grained materials, as composites and clays; and (f) to detect doping by certain ions, since the latter influences the unit cell

**Fig. 2.2** X-ray powder diffraction image (a); intensity of diffraction along any radius of the diffraction image (b)



parameters of the studied samples or induces change of crystal phase (Kapoor and Batra 2010). In recent years, modern powder diffraction is applied to determine the molecular structure of the material by the Rietveld method (Rietveld 1969). High-resolution synchrotron radiation data and new analysis procedures through suites of software (Toby 2001) have enhanced greatly the abilities of the method so that it has even entered in the field of molecular structure of proteins (Margiolaki and Wright 2008; Margiolaki et al. 2007).

Powder XRD is routinely used for characterization of materials, e.g., synthetic bio-inspired materials, since it gives a quick picture of the degree of resemblance to the prototype. The following is a useful example of its use: The size-controlled growth of hydroxyapatite (HA,  $\text{Ca}_{10}(\text{PO}_4)_6(\text{OH})_2$ ) nanocrystals, dispersed into a biopolymer matrix of chitosan (CTS, biocompatible, biodegradable, and bioactive, easily obtained from chitin) by coprecipitation, depends on the CTS/HA ratio. This is a biomimetic approach to engineer bone tissue (Rusu et al. 2005), since it is known that bone (such as long bone and jaw bone) is a biologically and chemically bonded composite between HA nanocrystals and type I collagen. Figure 2.3 shows how XRD has been used to determine the crystallinity and crystallite size of samples.

Crystallites size can be calculated by Scherrer's equation (Klug and Alexander 1974) [Eq. (2.1)]:

$$L = K \cdot \lambda / \beta_m \cdot \cos \theta \quad (2.2)$$

where  $L$  is the average crystallite size,  $\beta_m$  the full width of a diffraction order at half of the maximum intensity (in radians),  $\theta$  the Bragg angle of this diffraction order,  $\lambda$  the wavelength of X-ray radiation, and  $K$  is a constant related to the crystallite shape, approximately equal to unity. Note that  $\beta_m(\text{rad}) = \beta_m(\text{deg}) \cdot \pi/180$ . Crystallite size is used to compare the synthesized products with each other and compare them with the natural prototype.

The crystallinity degree,  $X_c$ , is expressed by the fraction of crystalline inorganic material in a sample. Since the amorphous material is formed at the expense of the crystalline phase, the intensity of a diffraction peak will be proportionately reduced upon loss of crystallinity. Therefore,  $X_c$  can be extracted from the XRD pattern of the partially crystalline sample as

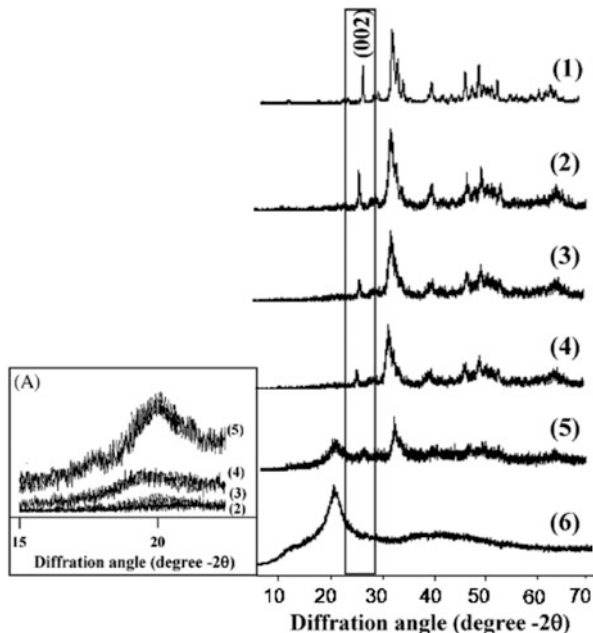


**Fig. 2.3** Powder XRD patterns of a series of composite samples of increasing CTS/HA ratio (2)–(5), HA (1), and CST (6). Based on them, it was shown that the higher the amount of CTS in a composite sample, the smaller the average crystallite size, the larger the percentage of nano-sized hydroxyapatite, and the more the composites' structural features resemble those of biological apatites. The *inset* (A) shows an enlarged selection area used to determine the XRD peak domain of CTS. The broad diffraction peak around  $2\theta$  20 is observed because CTS is a semicrystalline material. Reprinted from Biomaterials (Rusu et al. 2005). Copyright 2005 with permission from Elsevier

$$X_c = 1 - V_{mn}/I_n \quad (2.3)$$

where  $I_n$  is the intensity of an XRD peak and  $V_{mn}$  the intensity of the hollow between peak  $n$  and a neighboring peak  $m$  of close  $2\theta$  value (Kapoor and Batra 2010).

### 2.2.3 Small-Angle Scattering

Being a scattering and not a diffraction method, small-angle scattering (SAS) is used for low-order condensed matter, metal alloys, liquid crystals, and porous materials, powders, ceramics, synthetic polymers in solution and in bulk, and biological macromolecules in solution. It has been developed after the discovery by A. Guinier (Guinier and Fournet 1955) that scattering at very small angles  $\theta$  (close to the incident beam) is related to electron-density fluctuations of the

examined noncrystalline matter. Modern small-angle scattering by X-rays (SAXS) and neutrons (SANS) provide structural information not only (resolution one to a few hundred nm) on particle size and size distributions, shape, and orientation distributions but also on the internal low-resolution molecular structure of biological systems in the absence of single-crystals or structure of disordered and partially ordered systems (Svergun 2007). As SAXS has short response times, it can follow biological processes, which make it an ideal complement to time-consuming single-crystal diffraction method.

SAXS is used for structural studies of mesoporous materials, as zeolites and mesoporous silicas. These are products of self-assembly between organic surfactants and inorganic molecules that are organized like the liquid crystalline hexagonal, lamellar, or cubic phases. The structure-directing surfactant species are subsequently removed by calcination, leaving behind mesoporous rigid structures. The latter may exhibit uniform pores forming lattices with long-range organization, sometimes of high degree meaning that several Bragg reflections of the lattice can be identified, e.g., silica mesophases with highly ordered 2D hexagonal symmetry and a wide range of d-spacing (Zhao et al. 1998). The lattice spacing and the symmetry can be determined from the  $2\theta$  angles. Samples of low-degree order do not exhibit multi-peak patterns but single peaks, from which the pore size can be determined. Figure 2.4 shows the SAXS pattern of mesoporous functionalized aluminosilica films forming a long-range ordered cubic lattice (Athens et al. 2011). Note that the smaller  $2\theta$  angle, the larger the d-spacing.

### 2.2.4 Grazing Incidence X-Ray Diffraction

It is sometimes very difficult to analyze thin films due to their small diffracting volumes, which result in low diffracted intensities. The synchrotron technique of grazing incidence X-ray diffraction (GID) is a powerful tool for studying surfaces (Tanner et al. 2004). GID measurements are performed at very low incident angles to maximize the observed signal from the thin layers (Fig. 2.5). The intense synchrotron radiation and increased path length of the incident X-ray beam through the film result in increased intensity of the diffracted (or scattered) beam so that conventional analysis can be obtained.

An interesting example shows how, by SAXS grazing incidence X-ray diffraction (GID) experiment, it was possible to follow in real time the formation of highly oriented mesostructured silica films obtained by dip coating using cetyltrimethylammonium bromide (CTAB) as a templating agent and tetraethoxysilane (TEOS). This self-assembly complex process gives films with three different symmetries of the porous networks depending on the CTAB/TEOS molar ratio: 3D hexagonal (P63/mmc), cubic (Pm3n), and 2D hexagonal (p6m) (Grosso et al. 2002). The results were verified with transmission electron microscopy (see below).

A more complex application of GID is the study of the ordering influence of a freshly cleaved mica surface on surfactant tubular molecules (up to two layers)

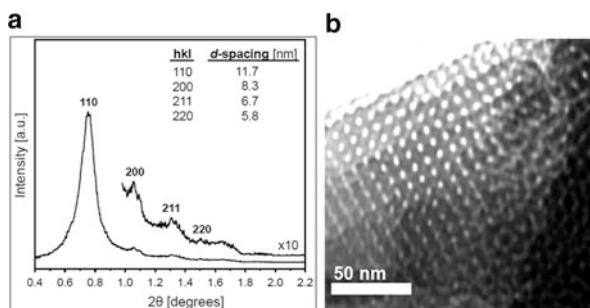


**Fig. 2.4** Small-angle X-ray scattering pattern for perfluorosulfonic acid-grafted cubic mesoporous aluminosilica film (a). The diffraction pattern is indexed to the body-centered-cubic (Im3m) structure. Transmission electron microscopy image (b). Reproduced by permission from Am. Chem. Soc. (Athens et al. 2011). Copyright 2011 Am. Chem. Soc.

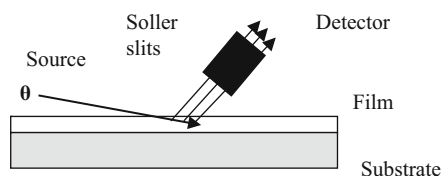


**Fig. 2.5** Schematic diagram of the geometry of grazing incidence X-ray diffraction

and subsequently on mesoscopic silica films grown on top from TEOS precursor (Aksay et al. 1996). Grazing incidence X-ray diffraction during growth revealed epitaxial alignment of the surfactant tubules with crystalline mica and significant strain on the silica overlayer. That is, mica forces the surfactant molecules to align parallel to the surface (by van der Waals or ionic forces) but exerts strain on the silica layer formed on top in the direction perpendicular to the surface and this strain is measured by GID as a 4 % distortion of the hexagonal packing of the mesophase silica. The strain on the surfaces of films seems to be released only if they are left to grow for a long period of time, after several surfactant-silica layers have been deposited.

### 2.2.5 Fiber Diffraction

The diffraction image of oriented fibers of hydrated B form of DNA (the famous Photo 51) taken by Rosalind Franklin in 1952, which has been a critical evidence in identifying the structure of DNA, is a well-known and characteristic fiber diffraction pattern. Fiber diffraction is obtained by other systems with one-dimensional periodicity, e.g., components of the cytoskeleton. The patterns



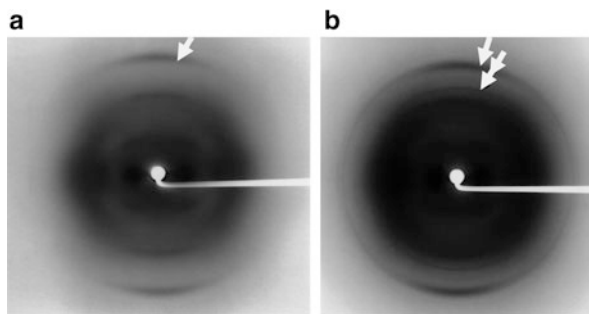
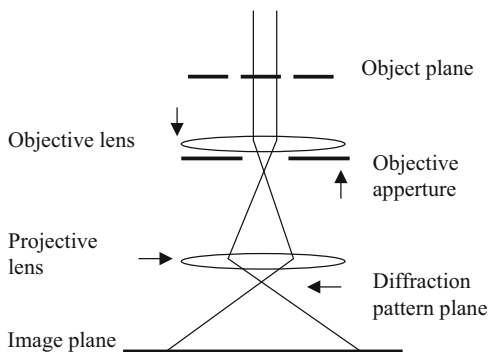


**Fig. 2.6** (a) X-ray diffraction pattern of an air-dried gelatin film under constant elongation (80 %). The vertical direction of the pattern coincides with the direction of elongation. The arrow indicates the collagen reflection corresponding to the periodicity of 0.29 nm. The 1.1 nm collagen reflection is oriented in the direction orthogonal to the stretching. (b) Under the same conditions, X-ray pattern from HA–gelatin film containing 9 % of inorganic phase under constant elongation (100 %). The arrow indicates the collagen reflection corresponding to the periodicity of 0.29 nm. The crooked arrow indicates the (0 0 2) HA reflection, corresponding to the periodicity of 0.344 nm. Reprinted from *Biomaterials* (Bigi et al. 1998). Copyright 1998, with permission from Elsevier

are obtained if oriented fibers with their axes parallel to each other are placed at right angles with respect to an X-ray beam. As in the case of DNA, a model of the fiber is constructed and its calculated fiber diffraction is compared to the observed.

Sometimes fiber diffraction is induced by external means on the examined samples, e.g., mechanically. Figure 2.6 shows diffraction images of films of gelatin–hydroxyapatite (HA) composites under mechanical stress (Bigi et al. 1998). Pure unstretched gelatin films exhibit an X-ray diffraction pattern of two complete rings corresponding to the characteristic periodicities of 0.29 and 1.1 nm. Upon stretching, the collagen molecules align their long axis parallel to the direction of deformation and the gelatin-layered structure becomes more ordered exhibiting fiber diffraction (Fig. 2.6, Left). The patterns from unstretched composite HA–gelatin films show the diffraction rings characteristic of gelatin (0.29 and 1.1 nm), as well as the rings of crystalline HA in agreement with a random distribution of the inorganic crystallites inside the disoriented gelatin. Under constant deformation, the fiber pattern (Fig. 2.6, right) displays the 0.29 nm collagen reflection along with the (0 0 2) HA reflection indicating that the orientations of the *c*-axis of the HA crystallites are preferentially oriented along the direction of elongation. Therefore, under deformation, the inorganic crystals, which are embedded in the gelatin layers, seem to squeeze out in the interlayer spaces and assume a preferred orientation parallel to the force trajectories.

**Fig. 2.7** Schematic diagram of the electron diffraction geometry



### 2.2.6 Electron Diffraction

Electron diffraction is similar to X-ray and neutron diffraction (Cowley 1992). Commonly, it is used for phase identification, lattice parameters and symmetry determination, and disorder and defect identification. Experiments are performed in a transmission electron microscope (TEM). Figure 2.7 shows a schematic diagram of TEM. Electrons are accelerated by an electrostatic potential before they interact with the object to be studied. By the interaction of the atomic potential of the object and the incident electron beam transmitted through it, diffracted electrons are generated that are focused into a regular arrangement of diffraction spots by an electromagnetic objective lens. The experimental setup allows for projection and collection of the electron diffraction pattern. Alternatively, if the diffracted waves and the transmitted beam interfere on the image plane, they form an enlarged image of the sample (TEM micrograph).

A great advantage of the transmission electron microscope is that by adjusting the electron lenses, it is possible to observe for the same region of a polycrystalline material both its electron microscope image (real space) and diffraction patterns (reciprocal space) as shown in Fig. 2.8. More importantly, it is possible to focus on very small areas, the size of a grain of the material, which can be a single crystal at specific orientation. Thus, the crystal lattices and orientation for all the crystalline grains can be determined. Therefore, it is possible to obtain the structural organization of a macroscopic sample by electron diffraction and TEM. This important advantage of electron diffraction derives from the fact that the scattering cross section of matter for electrons is  $10^3$ – $10^4$  times larger than that of X-rays and neutrons, with typical wavelengths ( $\sim 2 \times 10^{-12}$ ) one hundredth of the X-ray or neutron wavelength. Due to the large cross section, the electron beam can produce quite intense diffraction from extremely fine crystalline probe sizes (nm). By applying special geometry of the electron diffraction experiment, it is possible to collect 3D single-crystal diffraction data from a very small crystalline specimen and determine its molecular structure. Thus, recent highly improved electron diffraction techniques permit structure determination

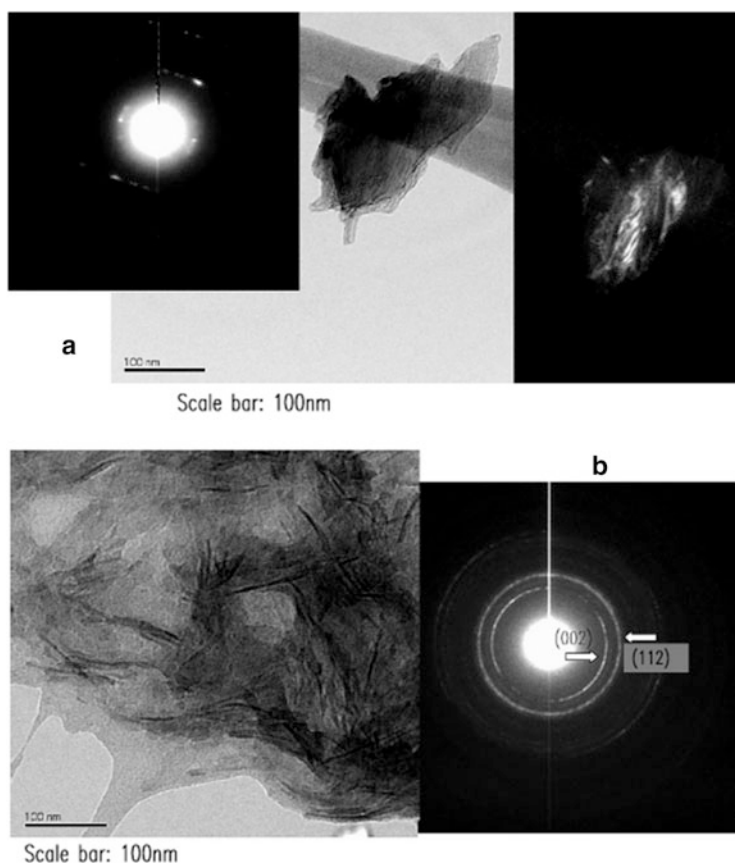


**Fig. 2.8** Electron diffraction patterns for organized gelatin (GEL)–HA nanocomposites (Chang et al. 2003) by a biomimetic chemical coprecipitation process strongly indicate the self-organization of well-developed HA nanocrystallites, embedded in GEL molecules (a). The electron diffraction of samples containing small amount of GEL shows discrete strong spots, almost like a single HA crystal, indicating a strongly preferred (0 0 2) orientation of HA crystals (and the higher orders (0 0 4), (0 0 6), and so on). The size of the tiny crystallites is quite big (30 nm × 70 nm, micrograph in (a)). This is suggested to result from a specific arrangement of reactive carboxylic groups of GEL that mimic the (0 0 2) planes of the HA crystal and induce its nucleation in nm crystallites from the stable aqueous solution that subsequently grow and fuse into single crystals. It is known that the (0 0 2) axis of HA nanocrystals in bone aligns with the collagen matrix (*c*-axis parallel with the COL fibers) (Chang et al. 2003). In contrast, as the amount of GEL added to the reaction is increased (b), the electron diffraction pattern is differentiated from the single-crystal diffraction spots to that of a polycrystalline sample with very sharp rings indicating growth of tiny nanocrystals. The crystallite size (5 nm × 14 nm micrograph in (b)) is smaller with relatively longer particles suggesting a preferred orientation quite unlike the crystal habit of pure HA. Reprinted from Biomaterials (Chang et al. 2003), Copyright 2003 with permission from Elsevier

for many materials for which the sizes are very small to allow for the usual single-crystal X-ray data collection, i.e., large complexes of macromolecules, nano-sized particles, and low-dimensional objects.

## 2.3 Microscopy

### 2.3.1 *Transmission Electron Microscopy*

As described above, TEM is the technique whereby a beam of electrons is transmitted through an ultrathin sample and diffracted (scattered) by its atomic potential. The diffracted (scattered) beam contains information about electron distribution in the sample that is used to form an image (Fig. 2.8). Thus, TEM gives the direct image of the sample, which frequently includes high-resolution imaging of the crystal lattice (Fig. 2.4). TEM's common uses have been to provide information (Wang et al. 2011) on shape and size of crystalline samples, e.g., nanocrystals and/or size of crystallites in amorphous samples, thus complementing the XRD results: For the CST/HA samples presented in Fig. 2.3 (Rusu et al. 2005), area domains from TEM micrographs were examined in order to find how many groups of crystallites with the same characteristic features existed (either particle length or width), and the percentage of crystallites in each population was determined. The analysis clearly confirmed the bimodal distribution of the HA crystallite length found by XRD, whose sizes are in the range of biological HA.

Modern transmission electron microscopes provide a range of complementary capabilities rendering the method of an analytical electron microscopy. There exist detectors that analyze inelastically scattered electrons (electron energy-loss spectroscopy, or EELS), excited electromagnetic waves (energy dispersion spectroscopy, EDS), and Z-contrast that provide information on chemical compositions and local atomic environments (Andre et al. 2011). As described in the electron diffraction section, these studies can be combined with elastic electron diffraction on extremely fine crystalline probes (nm). It is possible to generate 3D single-crystal diffraction data and hence the molecular structure of the material, a very important tool in developing structural models of multiple phase materials.

Electron diffraction and TEM are used to study the short-range order of amorphous solids. TEM is used to study transformations from an amorphous state to phases of increased structural organization of various materials or vice versa. Amorphous samples do not show distinct features in TEM because of lack of diffraction; thus, TEM is used to detect polycrystalline particles in amorphous matrices (Karavas et al. 2007). They are also used to see long-range orders, e.g., mesoporous silica (Grosso et al. 2002).

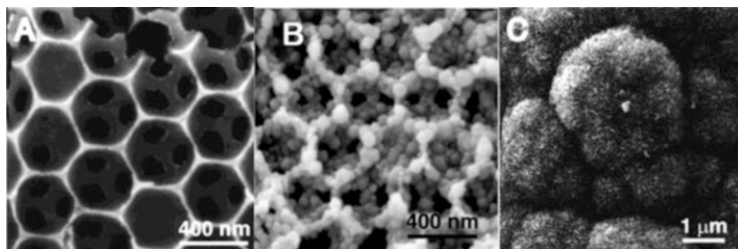


**Fig. 2.9** SEM micrograph of 3D structured macroporous bioglass (A), after immersion in simulated biofluids for 3 h (B) showing overgrowth of amorphous phosphate on the pore walls and after 4 days (C). Reproduced by permission from Chem. Mat. (Yan et al. 2001), Copyright 2001 Am. Chem. Soc.

### 2.3.2 Scanning Electron Microscopy

SEM images a sample by scanning it with a beam of electrons which interact with atoms at or near the surface of a sample producing signals that contain information about the sample's surface structure, composition, and electrical conductivity. In contrast to TEM, it is using detectors placed before the sample on the same side of the incident electron beam (in Fig. 2.7) and does not require thin samples. Due to the very narrow electron beam, SEM micrographs have a large depth of field yielding a characteristic three-dimensional appearance (Fig. 2.9) that provides information on crystal shape, particle size, and the surface topography (Yan et al. 2001).

For conventional SEM imaging, the specimens must be electrically conductive in order to prevent the accumulation of electrostatic charges; therefore, they are usually coated with a thin layer of electrically conducting material (gold, platinum, gold/palladium alloy, osmium, chromium, graphite, and others). Alternatively, environmental SEM (ESEM) can be used (low-voltage mode), where the working distance is short and the specimen is placed in a relatively high-pressure chamber that helps to neutralize charges. In the standard detection mode by the method of secondary electron imaging (SEI, resolution less than 1 nm), steep surfaces and edges appear brighter than flat surfaces, which results in images with a well-defined, 3D appearance. The backscattered electrons (BSE) mode (electrons are reflected out of the specimen) is used to detect contrast between areas with different chemical compositions, because the intensity of electron backscattering depends on the atomic number of the atoms.

### 2.3.3 Confocal Scanning Laser Microscopy

Confocal scanning laser microscopy (CSLM) reconstructs 3D images of the specimen by assembling a series of thin slices, up to 100  $\mu\text{m}$ , taken along an axis perpendicular to the slices (Semwogerere and Weeks 2005). CSLM scans point by

point via 3–5 laser systems and combines the images of the slices by electronic means similar to those used in SEM to create the overall picture. Confocal microscopes image either by reflecting light off the specimen or by inducing fluorescence from fluorophores applied to the specimen (Andre et al. 2011).

### 2.3.4 Atomic Force Microscopy

Atomic force microscopy (AFM) is a very versatile method of nano-science used for (a) imaging (resolution of the order of nm), (b) measuring forces, and (c) manipulating molecules on surfaces. AFM operates by a fine tip (cantilever) that scans a surface and “feels” the forces from the sample. Depending on the mode, the measured forces include mechanical contact force, van der Waals forces, capillary forces, chemical bonding, electrostatic forces, and magnetic forces. In contrast to the electron microscopes (TEM, SEM), AFM does not require vacuum; it can be used at ambient conditions and in liquid samples; therefore, it is suitable for biological systems. Since AFM’s resolution is very high, it is used complementary to TEM and SEM methods to provide the 3D profile of surfaces (Andre et al. 2011). Sometimes it can reveal details undetectable with high-resolution SEM, e.g., AFM revealed the presence of nanoparticulate silica organized around the central axial filament of freshly cleaved (un-etched) spicule cross sections (Weaver et al. 2003). AFM is commonly used to image roughness, epitaxial deposition, grain size, study the morphology (or symmetry) of a growing overlayer on substrates of various symmetries in order to examine the influence of the latter (Aksay et al. 1996), monitor phase changes, and so on.

## 2.4 Spectroscopy

### 2.4.1 Infrared Spectroscopy (IR)

IR is usually used as absorption spectroscopy at the  $4,000\text{--}400\text{ cm}^{-1}$  range, where vibrational or rotational–vibrational excitation of covalently bonded atoms and groups takes place. The IR absorbance frequencies are characteristic of the chemical groups and their chemical environment; thus, the spectrum can be used as a fingerprint for identification of unknown compounds or to judge about close intermolecular interaction of specific groups. For example, changes in the absorption frequencies of the spectrum are correlated to changes in the environment of an atom and emergence of new peaks to new covalent bond formation. The following are some characteristic examples: (a) IR has been employed to examine the propensity of a three-dimensionally ordered macroporous bioactive glass for apatite formation by soaking in simulated body fluid at body temperature. During the

soaking, the growing of the absorptions due to phosphate (mainly the low-intensity band at  $567\text{ cm}^{-1}$  corresponding to the antisymmetric vibrational mode of P-O in amorphous calcium phosphate) and carbonate groups could be observed close to the Si peaks (typical bands at the low-wave number range the  $1,080$ ,  $800$ , and  $470\text{ cm}^{-1}$  corresponding to the asymmetric Si-O-Si stretch, the symmetric Si-O-Si stretch, and the Si-O-Si deformation mode, respectively). The growing of the peak corresponding to phosphates suggested that deposition of amorphous calcium phosphate was taking place (Yan et al. 2001). (b) In the gelatin (GEL)-hydroxyapatite (HA) composite (Chang et al. 2003), FTIR analysis showed a red shift of the band at  $1,339\text{ cm}^{-1}$  for a series of HA-GEL composites attributed to the covalent bond formation of gelatin with  $\text{Ca}^{2+}$  ions of HA nanocrystals. This band characterizes the wagging vibration of proline side chains of GEL (as in collagen). (c) In the micro-FTIR study of the chemical structure of synthesized silk/silica hybrids by the sol-gel process in the presence of a cross-linking agent, two new peaks at  $1,469\text{ cm}^{-1}$  and  $958\text{ cm}^{-1}$  emerge that are ascribed to the group  $\text{-N=C-}$  of the cross-linking agent showing that the latter is able to form covalent bonds between silk and sol-gel dispersion particles (Hou and Chen 2010).

### 2.4.2 Raman Spectroscopy

As IR spectroscopy, Raman spectroscopy is used to study low-frequency modes of a molecular system, as vibrational or rotational, in the solid state. It is based on Raman scattering, a scattering that results from interaction of IR radiation with vibrational modes of the examined molecular system. A vibrational spectrum may be obtained from Raman scattering that yields similar, but complementary, information to IR spectroscopy. In materials science the 2D micro-Raman spectroscopy is very helpful, because it maps the surface of the sample and provides a chemical characterization at every point: In a study that examined whether a poorly water-soluble drug dispersed in a polymeric matrix exist in the form of amorphous nano-dispersions or is molecularly dispersed, it was revealed by SEM and TEM that the drug forms amorphous nano-dispersions into the polymer matrix. However, it was found by micro-Raman mapping of the whole surface that some portion of the drug exists also as molecular dispersion inside the amorphous polymer matrix (Karavas et al. 2007).

### 2.4.3 Nuclear Magnetic Resonance Spectroscopy

Solid-state nuclear magnetic resonance (NMR) provides the same type of information as NMR spectroscopy in solution, but special equipment and methods (including magic angle spinning and cross polarization) are needed due to anisotropic or orientation-dependent interactions in the solid state (Laws et al. 2002). Since silicon

and phosphorous, as well as hydrogen and carbon, have isotopes with a spin of  $\frac{1}{2}$ , solid-state NMR can provide information on the intermolecular interactions of these atoms that are common composite inorganic biomaterials. Therefore, it provides information on covalent and intermolecular interactions and contributes to build indirectly a model of the structure of the material, as in the case of IR spectroscopy. Thus, single-pulse  $^{29}\text{Si}$  magic angle spinning NMR spectra of siliceous spicules isolated from *T. aurantia* heated to 300 and 600 °C revealed different degrees of heat-induced silica condensation. The results show that the inorganic silica framework is moderately condensed, even in the non-heat-treated sample (Weaver et al. 2003). Another application, by  $^{29}\text{Si}$  NMR spectra, is the determination of the proportions of Qn species (Qn representing a Si atom bonded to n other Si atoms via O-bridges, e.g., Q3 and Q4) allowing the quantification of the cross-linking degree of silica (Hou and Chen 2010).

## 2.5 Thermal Analysis

Thermal analysis monitors the thermal response of the systems on heating and measures the energy released or absorbed (exothermic or endothermic); thus, it can investigate the mechanisms of thermal processes of a system. Thermal behavior gives indirect information on the examined structure and complements results from other methods. Both thermal analysis techniques, *differential thermal/thermogravimetric analysis* (DT/TGA) and *differential scanning calorimetry* (DSC), are usually applied in the thermal analysis. DT/TGA measures the weight loss of the samples upon heating, which it is usually interpreted as due to either elimination of water or to degradation and loss of the organic matter. DSC can detect the above, as well as monitor possible structural modifications and phase changes and measure the energetics involved.

Examples are as follows: (a) DT/TGA and DSC measurements in sponge spicules (Croce et al. 2004) indicate the presence of organic matter and its degradation, which takes place with weight loss at high temperature. At low temperature endothermic effects in DSC are either due to loss of coordinated water to protein molecules in the spicules or structural changes of the proteins. The kinetics of DSC provide information on the efficiency of the energy transfer from the instrument furnace to the organic matter located within the spicule cavity, therefore on the thickness of the walls of the silica matrix, which is different for the various species studied. (b) DT/TGA was employed to determine the phase stability and the reaction temperatures during the fabrication of Mg-substituted tricalcium phosphate scaffolds by solid-state reaction processes in various studies for biomimetic bone regeneration (Zhang et al. 2009). (c) The study of organized gelatin [GEL]/HA nanocomposites (Chang et al. 2003) strongly supports the existence of a chemical bond between HA and GEL in the composite. DT/TGA data for certain [GEL]/HA ratios showed similar results to real bone.



## 2.6 Concluding Remarks

The analysis of such complex structures as inorganic biomaterials requires the use of various complementary techniques. As a concluding example, the structural study of intact spicules from various species of sponges is presented. It was carried out with a selected combination of methods, SEM, thermogravimetric and calorimetric analysis, IR spectroscopy, fiber diffraction, and theoretical molecular modeling (Croce et al. 2004). The axial filament composed of proteins and positioned at the spicule axis is crucial to the spicule formation because it functions as template for silica deposition. Both mega- and microscleres spicules of hexactinellid *S. joubini* and the demosponges *G. cydonium*, *P. ficiformis*, and *T. aurantium* were used in the study. The above combination of techniques allowed the analysis of the axial filaments inside their natural siliceous case, which give a more realistic picture of their organization, in contrast to structural characterization carried out on filaments extracted by strong treatment (Shimizu et al. 1998) that may have caused denaturation or structural changes in the proteins.

SEM with energy dispersive spectrometry (EDS) analysis indicated that in all samples, the inorganic envelope is composed almost exclusively of silica (Si and O). In megascleres, the presence of cavities was revealed. These cavities are the sites where the proteins responsible for the spicule growth are hosted (*vide infra*). The thermal analysis showed that for *S. joubini* (a) the overall energy involved during the heating is significantly larger than in the other spicules and (b) the onset of the temperature process is at lower temperature. These observations have been interpreted as deriving from greater amount of biomolecules in the axial filament of the hexactinellid species and that the biomolecules are less tightly bound. FTIR spectroscopy was employed to characterize the surface of siliceous materials, in particular to evaluate the presence of both surface hydroxyls and organic molecules, with particular interest to the spicule proteins. The fact that the band at  $3,680\text{ cm}^{-1}$ , attributable to the stretching modes of Si–OH groups of the inorganic matrix, becomes evident upon evacuation at  $250\text{ }^{\circ}\text{C}$  indicates that these –OH groups at room temperature must be strongly involved in hydrogen bond interactions with the organic matter. FTIR spectroscopy showed also evidences of beta-sheet structures in the analyzed spicule proteins. Synchrotron radiation fiber diffraction experiments on intact spicules gave a more realistic picture of the protein organization. The sharp diffraction spots obtained from bundles of well-aligned fibers indicated that the protein units forming the axial filaments inside the spicules must be highly organized. In the planes perpendicular to the spicule axis, the protein units appear to be packed in a compact hexagonal way (Fig. 2.10a) with repeat distances 5.8 nm for demosponge spicules (*T. aurantium*, *G. cydonium*, and *P. ficiformis*) and 8.4 nm for the hexactinellid *S. joubini*. These distances were calculated from the

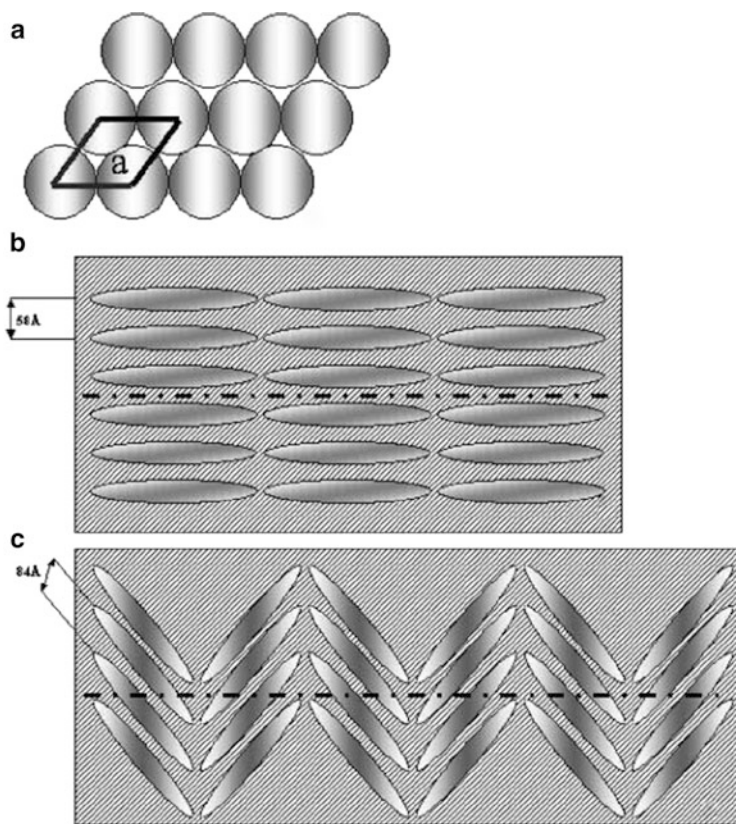


**Fig. 2.10** 2D hexagonal packing (a); structural model of the organization of the filaments in *G. cydonium* spicules (b); structural model of the organization of the filaments in *S. joubini* spicules (c). The dot and dash lines represent the longitudinal axis of the filament. Reprinted from Biophys J (Croce et al. 2004), Copyright 2004 with permission from Elsevier

position and distribution of the spots in the fiber diffraction (Croce et al. 2003). Equatorial spots up to the third order of *G. cydonium* spicules are consistent with a very regular hexagonal arrangement of protein units aligned along the spicule axis (Fig. 2.10b). The presence of nonequatorial spots in the diffraction patterns of *S. joubini* suggests also a hexagonal packing but of spirally oriented protein units along the spicule axis, according to the 2D model of (Fig. 2.10c). The diffraction spots in all patterns are much sharper than one would normally expect from a fiber, and this feature has been explained by the authors by the assumption that the silica present in the axial filament is organized around the protein units as a highly ordered mesoporous material and is embodying the protein units in regular mesoporous scaffolding.

## References

- Aksay IA, Trau M, Manne S, Honma I, Yao N, Zhou L, Fenter P, Eisenberger PM, Gruner SM (1996) Biomimetic pathways for assembling inorganic thin films. *Science* 273:892–898
- Andre R, Tahir MN, Link T, Jochum FD, Kolb U, Theato P, Berger R, Wiens M, Schroeder H-C, Muller WEG et al (2011) Chemical mimicry: hierarchical 1D TiO<sub>2</sub>@ZrO<sub>2</sub> core-shell structures reminiscent of sponge spicules by the synergistic effect of silicatein-r and silintaphin-1. *Langmuir* 27:5464–5471
- Athens GL, Kim D, Epping JD, Cadars S, Ein-Eli Y, Bradley FC (2011) Molecular optimization of multiply-functionalized mesoporous films with ion conduction properties. *J Am Chem Soc* 133:16023–16036
- Bigi A, Panzavolta S, Roveri N (1998) Hydroxyapatite-gelatin Plms: a structural and mechanical characterization. *Biomaterials* 19:739–744
- Blow DM (2002) Outline of crystallography for biologists. Oxford University Press, Oxford
- Chang MC, Ko CC, Douglas WH (2003) Preparation of hydroxyapatite—gelatin nanocomposites. *Biomaterials* 24:2853–2862
- Cowley JM (ed) (1992) Electron diffraction techniques. International Union of Crystallography, Oxford University Press, Oxford
- Croce G, Frache A, Milanesio M, Viterbo D, Bavestrello G, Benatti U, Giovine M, Amenitsch H (2003) Fiber diffraction study of spicules from marine sponges. *Microsc Res Tech* 62:378–381
- Croce G, Frache A, Milanesio M, Marchese L, Causá M, Viterbo D, Barbaglia A, Bolis V, Bavestrello G, Cerrano C et al (2004) Structural characterization of siliceous spicules from marine sponges. *Biophys J* 86:526–534
- Fischer E (1894) Einfluss der configuration auf die Wirkung der enzyme. *Ber Deutsch Chem Ges* 27:2985–2993
- Grosso D, Babonneau F, Albouy P-A, Amenitsch H, Balkenende AR, Brunet-Bruneau A, Rivory J (2002) An in situ study of mesostructured CTAB-silica film formation during dip coating using time-resolved SAXS and interferometry measurements. *Chem Mater* 14:931–939
- Guinier A, Fournet G (1955) Small-angle scattering of X-rays. Wiley, New York
- Hou A, Chen H (2010) Preparation and characterization of silk/silica hybrid biomaterials by sol-gel crosslinking process. *Mat Sci Eng B* 167:124–128
- Karavas E, Georgarakis M, Docoslis A, Bikiaris D (2007) Combining SEM, TEM, and micro-Raman techniques to differentiate between the amorphous molecular level dispersions and nanodispersions of a poorly water-soluble drug within a polymer matrix. *Int J Pharm* 340:76–83
- Kapoor S, Batra U (2010) Preparation and bioactivity evaluation of bone like hydroxyapatite - bioglass composite. *Int J Chem Biol Engin* 3:13, 24–28
- Klug HP, Alexander LE (1974) X-ray diffraction procedures for polycrystallite and amorphous materials, 2nd edn. Wiley, New York
- Laws DD, Bitter H-ML, Jerschow A (2002) Solid-state NMR spectroscopic methods in chemistry. *Angew Chem Int Ed* 41:3096–3129
- Lehn J-M (1995) Supramolecular chemistry. VCH, Weinheim
- Margiolaki I, Wright JP, Wilmanns M, Fitch AN, Pinotsis N (2007) Second SH3 domain of ponsin solved from powder diffraction. *J Am Chem Soc* 129:11865–11871
- Margiolaki I, Wright JP (2008) Powder crystallography on macromolecules. *Acta Cryst A* 64:169–180
- Rietveld HM (1969) A profile refinement method for nuclear and magnetic structures. *J Appl Cryst* 2:65–71
- Rusu VM, Ng C-H, Wilkec M, Tierscha B, Fratzld P, Peter MG (2005) Size-controlled hydroxyapatite nanoparticles as self-organized organic–inorganic composite materials. *Biomaterials* 26:5414–5426
- Semwogerere D, Weeks ER (2005) Confocal microscopy. In encyclopedia of biomaterials and biomedical engineering. Taylor & Francis, London

- Shimizu K, Cha J, Stucky GD, Morse DE (1998) Silicatein a cathepsin L-like protein in sponge biosilica. *Proc Natl Acad Sci USA* 95:6234–6238
- Svergun DI (2007) Small-angle scattering studies of macromolecular solutions. *J Appl Crystallogr* 40:s10–s17
- Tanner BK, Hase TPA, Lafford TA, Goorsky MS (2004) Grazing incidence in-plane X-ray diffraction in the laboratory. *Adv X-Ray Anal* 47:309–314
- Toby BH (2001) EXPGUI, a graphical user interface for GSAS. *J Appl Cryst* 34:210–213
- Wang G, Peng Q, LI Y (2011) Lanthanide-doped nanocrystals: synthesis, optical-magnetic properties, and applications. *Acc Chem Res* 44:322–332
- Weaver JC, Pietrasanta LI, Hedin N, Chmelka BF, Hansma PK, Morse DE (2003) Nanostructural features of demosponge biosilica. *J Struct Biol* 144:271–281
- Yan H, Zhang K, Blanford CF, Francis LF, Stein A (2001) In vitro hydroxycarbonate apatite mineralization of CaO-SiO<sub>2</sub> sol-gel glasses with a three-dimensionally ordered macroporous structure. *Chem Mater* 13:1374–1382
- Zhang X, Takahashi T, Vecchio KS (2009) Development of bioresorbable Mg-substituted tricalcium phosphate scaffolds for bone tissue engineering. *Mat Sci Eng C* 29:2003–2010
- Zhao D, Feng J, Huo Q, Melosh N, Fredrickson GH, Chmelka BF, Stucky GD (1998) triblock copolymer synthesis of mesoporous silica with periodic 50 to 300 Angstrom pores. *Science* 279:548–552

Biomedical Inorganic Polymers

Bioactivity and Applications of Natural and Synthetic

Polymeric Inorganic Molecules

Müller, W.E.G.; Wang, X.; Schröder, H.C. (Eds.)

2013, X, 303 p. 91 illus., 50 illus. in color., Hardcover

ISBN: 978-3-642-41003-1